HURRICANE-GENERATED WIND-WAVE RESEARCH AT NOAA/NCEP [1]

Jose-Henrique G.M. Alves[2,3],
Hendrik L. Tolman[2,4] and Yung Y. Chao[5]

NOAA/NCEP/EMC
Marine Modeling and Analysis Branch
Camp Springs, Maryland, USA

1 INTRODUCTION

Improving the forecasts of hurricane-generated waves is an essential step toward minimizing the damage caused by tropical storms to coastal settlements and economic activities in the nearshore zone. NOAA's National Centers for Environmental Prediction (NCEP) has pioneered this field through the implementation of two specialized hurricane-generated wave models, which currently provide regional forecasts in the north Atlantic and Pacific ocean basins.

NCEP has been continuously broadening its research efforts in the field. Focus has recently been placed not only on increasing the quality of operational hurricane-generated wave model products, but on providing forecasters with practical tools for estimating maximum hurricane-generated waves. This manuscript presents a summary of some recent results from activities related to hurricane-generated wave research conducted at NCEP.

In the first part of the manuscript, we examine the skill of operational forecasts and hindcasts made with NCEP's hurricane-generated wave model NAH (North Atlantic Hurricane). Wave model predictions are validated against buoy and altimeter data measured during hurricanes Isidore and Lili (2002) and Isabel (2003).

In the second and final part, we describe the applications of a version of WAVEWATCH III featuring a movable spatial grid. First, the moving grid model is used to investigate the impact of space-time interpolation of storm winds to wave forecasting. Finally, the moving grid model is used to investigate a new parameterization for predicting hurricane-generated maximum wave heights.

2 OPERATIONAL FORECASTS

Operational wind-wave forecasts issued by the US National Weather Service are made using the NOAA WAVEWATCH III (NWW3) Wave Model Suite (Tolman et al., 2002). This system consists presently of four core wave model implementations and two specialized hurricane wave models, covering the global ocean and focusing on three regions in which NWS has forecast responsibilities: the Western North Atlantic (WNA), the Eastern North Pacific (ENP) and the Alaskan waters (AKW) models. The WNA and ENP grids are shared by two specialized models, the North Atlantic and North Pacific hurricane wave model, NAH and NPH.

Most wave models in the NWW3 suite are forced with wind fields from NCEP's global atmospheric model GFS. The GFS model, however, has limited skill in depicting properly hurricane surface winds, due to its low spatial resolution and other limitations of its current implementation. Since a wave model can only be as good as the winds that drive it, complexities of small-scale hurricane wind field variability must be specified using higher-resolution surface wind fields.

High-resolution forecasts of hurricane winds are generated at NCEP by the GFDL model. Storm-centered GFDL model runs target individual hurricanes in grids that many times do not cover the en-

[1] MMAB contribution Nr. 242
[2] SAIC/GSO
[3] E-mail:Henrique.Alves@noaa.gov
[4] E-mail:Hendrik.Tolman@NOAA.gov
[5] E-mail:Yung.Chao@NOAA.gov

tire wave model domain. In association with the frequent existence of multiple hurricanes, this requires the blending of an arbitrary number of available GFDL wind fields with flows outside the hurricane-dominated area, obtained from the GFS model. Details of the blending scheme currently used operationally are provided in Chao et al. (2004).

An example of the effectiveness of using higher-resolution winds blended to GFS data to represent multiple hurricane surface wind fields is given in Figure 1, showing wave height fields during hurricanes Jeanne and Karl (2004). The differences between wave field simulations from the WNA and NAH models in the hurricane-dominated area are striking. Preliminary comparisons with measured data from those two events reveal that the NAH model provides more accurate predictions of wave height, and more precise positioning of maximum wave-height regions in both hurricane wave fields.

The NAH model was implemented on May 2001. Since then, the NAH model has provided a representative range of hurricane-generated wave forecasts, which have allowed several validation tests to be performed. Consequently, these specialized models have undergone several improvements, and are continuously upgraded to include new features as new case studies become available. In this section we present an overview of the most relevant findings of validation studies carried out for hurricanes Lili and Isidore (2002) and Isabel (2003).

2.a Hurricanes Isidore and Lili

Hurricanes Isidore and Lili had a devastating impact in areas near the Gulf of Mexico, both occurring between September 18th and October 7th 2002. A comprehensive evaluation of model performance during these two events, made relative to NDBC buoy data, is presented in Chao et al. (2004). Here we provide a summary of their main results, which focus on wave hindcasts and forecasts up to a 72h horizon.

Table 1 contains bulk validation statistics of wind intensity U_{10} and wave field parameters H_s and T_p from WNA and NAH wave model hindcasts, relative to measurements made at eight NDBC/NOAA buoys. The differences between NAH and WNA model hindcasts during Isidore and Lili are relatively modest. WNA slightly outperforms NAH at most buoys, which, except for buoy 42001, are located away from the tracks of hurricanes Isidore and Lili. Buoy 42001, however, was directly under Lili's track. Therefore, it has great importance in our evaluation because it was the only buoy exposed to extreme wind intensities during these two hurricanes. Validation statistics at this location indicate a clear superiority of NAH model predictions in terms of wave heights.

Most other buoy sites were far from the tracks of Isidore and Lili. Therefore, the relatively better performance of the WNA model is related to the arrival of swells generated by the hurricanes. A comparison between model winds and surface wind analyses for Isidore and Lili, made available by the Hurricane Research Division of NOAA (see Chao et al., 2004), suggested that the GFDL model systematically underestimated surface winds outside the maximum wind region (the outer flow). In con-

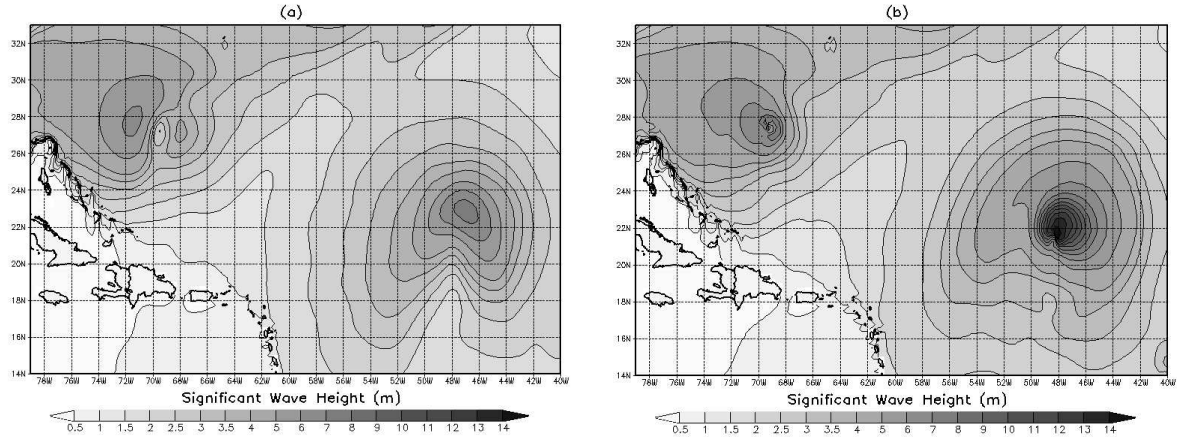

Fig. 1: Significant wave heights from (a) the WNA and (b) the NAH models for hurricanes Jeanne and Karl (Sep 2004)

trast, GFS winds slightly overestimated the analyzed winds in the outer flows of both hurricanes.

Table 1: Bulk validation statistics for the combined occurrence period of hurricanes Isidore and Lili. WNA and NAH wave model results are compared to observations at eight NDBC buoy locations. [Adapted from Chao et al., 2004]

		U_{10}				H_s			
Buoy	Model	Bias (m/s)	RMS (m/s)	SI	r	Bias (m)	RMS (m)	SI	r
42001	WNA	-0.29	2.95	0.36	0.82	0.17	0.60	0.32	0.94
	NAH	-0.16	1.61	0.20	0.95	0.13	0.46	0.24	0.97
42002	WNA	-0.35	1.50	0.19	0.91	-0.08	0.27	0.15	0.98
	NAH	-0.38	1.65	0.21	0.89	-0.17	0.30	0.14	0.98
42003	WNA	0.33	1.29	0.15	0.96	0.08	0.37	0.18	0.97
	NAH	-0.07	1.28	0.16	0.95	-0.13	0.56	0.27	0.93
42039	WNA	0.42	1.25	0.18	0.96	0.02	0.30	0.18	0.98
	NAH	0.09	1.26	0.19	0.95	-0.12	0.35	0.20	0.98
42040	WNA	0.83	1.40	0.16	0.98	0.06	0.30	0.17	0.99
	NAH	0.40	1.21	0.17	0.97	-0.11	0.33	0.18	0.98
42019	WNA	0.50	1.09	0.14	0.95	-0.16	0.49	0.32	0.94
	NAH	0.49	1.15	0.15	0.94	-0.21	0.51	0.32	0.95
42020	WNA	-0.03	0.98	0.15	0.94	-0.24	0.49	0.28	0.93
	NAH	-0.03	1.12	0.17	0.92	-0.29	0.49	0.26	0.95
42036	WNA	0.69	1.48	0.21	0.94	0.01	0.23	0.16	0.98
	NAH	0.30	1.39	0.22	0.92	-0.12	0.29	0.19	0.97

A qualitative analysis of fetch dimensions during Isidore and Lili shows that outer flows are a very important source of swells, due to the extent and persistence of moderately strong winds. Swells from the NAH model were, therefore, systematically lower than WNA swells, due to the poorer performance of the GFDL model in representing winds in the outer flow. This explains the relatively better performance of the WNA model at most buoys, since most buoy sites were far from both hurricane's tracks, i.e. exposed only to swell systems.

The underestimation of outer-flow surface winds in the GFDL model resulted from deficiencies in the planetary boundary layer (PBL) closure scheme used in that model until the end of the 2002 hurricane season. To alleviate this deficiency, the PBL scheme used in the GFS model was implemented onto the GFDL model before the 2003 season (Tim Marchock, personal communication, 2004). Results presented below for hurricane Isabel indicate that these changes in the PBL scheme of the GFDL model have reduced the problem, with the benefit of improving the skill of the NAH model in predicting swell systems.

Extreme hurricane-generated sea states are generally a greater concern for weather forecasting. The performance of the WNA and NAH models in terms of predicting extreme sea states is summarized in Figure 2. These "target" plots illustrate the bias of model predictions of maximum H_s relative to buoy data, indicating as well the time lag between model and measurements for the occurrence of the storm peak. Shaded areas in the figure outline acceptable ranges of H_s bias and time lags, set at $\pm$ 20 % and $\pm$ 3 h, respectively.

Figure 2 shows target plots for maximum waves, which occurred during hurricane Lili, at the following forecast ranges: -6h-0h, 0h-12h, 12h-24h and 36h-48h. Predictions of storm maxima from the NAH model generally fell within or near the acceptable $\pm$ 3-hour range out to the 48h forecast horizon. Time lags from the WNA model predictions were also mostly on target, except at two buoy locations (42019 and 42020) with lags clearly falling outside the tolerance bounds.

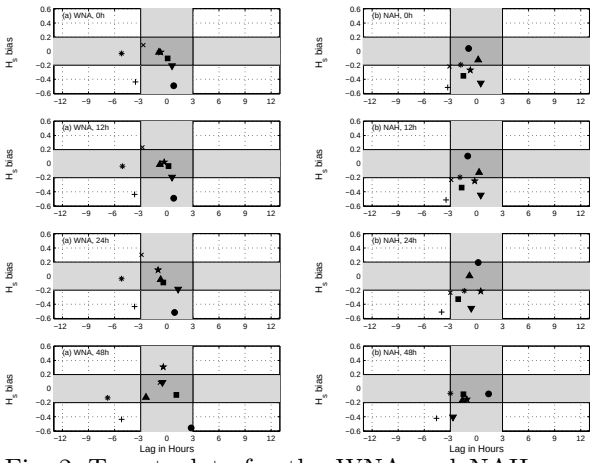

Fig. 2: Target plots for the WNA and NAH models indicating accuracy for predicting maximum H_s during hurricane Lili. Buoys: 42001 (•), 42001 (▲), 42003 (■), 42039 (★), 42040 (×), 42019 (+), 42020 (∗) and 42036(▼). [Adapted from Chao et al., 2004.]

In terms of maximum H_s biases, target plots seem to indicate that WNA and NAH models had similar general performance. Most data points, however, refer to swell waves generated by Lili. The only location that was directly exposed to actual extreme waves actively generated within the hurricane's maximum wind region was buoy 42001. Measured maximum H_s at this location of H_s=11.2 m was very closely reproduced by the NAH model's hindcast and forecasts up to 48h. In contrast, WNA model hindcast and forecasts significantly underestimated maximum H_s at this buoy location.

2.b Hurricane Isabel

Hurricane Isabel crossed the North Atlantic in September 2003, making landfall in the North Carolina coast. During its long life cycle, Isabel transitioned from a compact category 5 hurricane to a large category 2 hurricane, near landfall. This hurricane became a very powerful study case, due to the availability of a vast database of satellite, aircraft and surface buoy measurements. A detailed evaluation of the NAH model using such database is presented in Tolman et al. (2004a,b). Here we provide a summary of their main findings.

Isabel's region of maximum H_s was sampled several times by the altimeter on-board the satellite Jason-1. Data corresponding to two satellite crossings are shown in Figure 3. The upper panels in this figure illustrate a satellite crossing at an early stage of Isabel's life cycle. At this stage the storm was a very compact, category 5 hurricane. Lower panels show Isabel, then a much larger category 2 hurricane, near landfall.

Despite satellite quality-control drops near the most extreme conditions, remaining co-locations shown in the upper right-hand panel in Figure 3 reveal a very good agreement between NAH simulations and altimeter data. On the other hand, WNA models results fall much below Jason's measurements. These results illustrate the severe limitations of the GFS model in representing properly the structure of a very compact and intense hurricane. On the other hand, they strongly support the need for higher resolution winds in hurricane-generated wave models.

Lower panels in Figure 3 show that as Isabel grew in size and reduced its intensity, the limitations of the GFS model were attenuated. These changes led to a very good performance of both WNA and NAH models in reproducing the altimeter measurements of H_s. The skill of both wave models was high enough to capture even finer details of the observed wave field, such as the drop in wave height values near the eye of the hurricane.

Several NDBC/NOAA buoys deployed in the North Atlantic provided measurements of wave fields generated by Isabel. Since most buoys are located near the coast, they were mostly exposed to windseas generated during latter stages of Isabel's life cycle or swells. Therefore, buoy measurements of Isabel's maximum wave height generally confirm the good performance of both wave models. In most cases, however, buoy data reveal that swell fields gener-

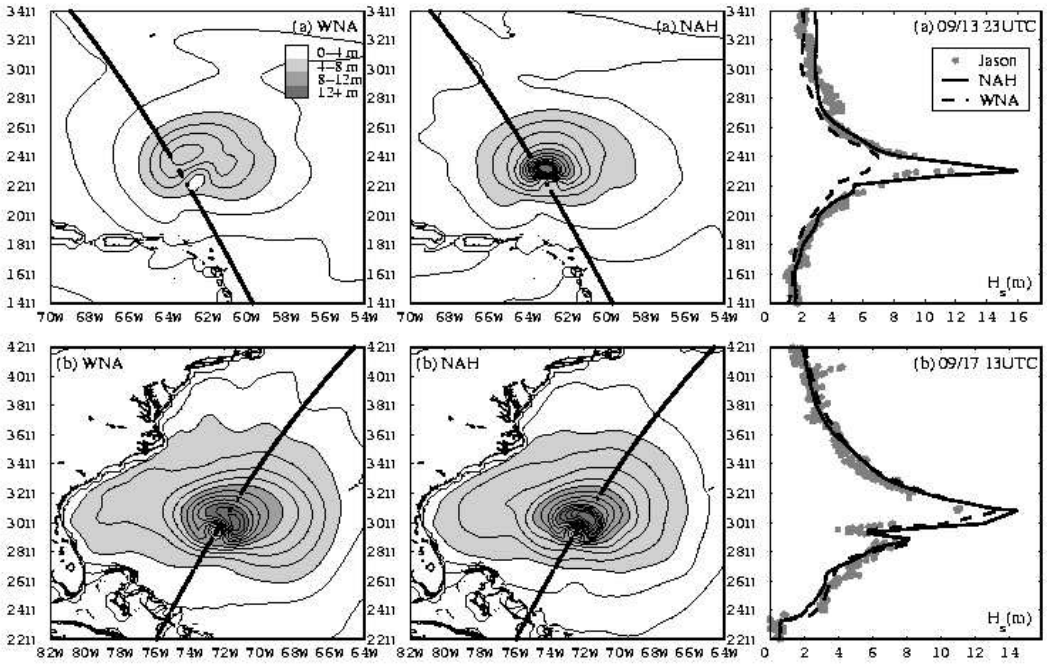

Fig. 3: Significant wave heights H_s (m) from the WNA (left) and the NAH (middle) models, plotted with Jason-1 tracks on (a) 9/13 2300 UTC and (b) 9/17 1300 UTC. Co-located along-track H_s from NAH and WNA vs. altimeter data (gray circles). [Adapted from Tolman et al., (2004a,b)]

ated during the hurricane's earlier life stages were generally underestimated by both NAH and WNA models.

Despite the generally poor prediction of swell fields generated in the earlier life stages of Isabel by both NAH and WNA wave models, Figure 4 indicates that the NAH model predicted the hurricane's swell fields more accurately. This figure shows time series of one-dimensional wave energy spectra versus frequency at NDBC/NOAA buoy 44018, located to the north of Isabel's track. The arrival of swell events is well-marked in the diagrams, appearing as slanted wave-energy ridges indicating a reduction of spectral peak frequency with time.

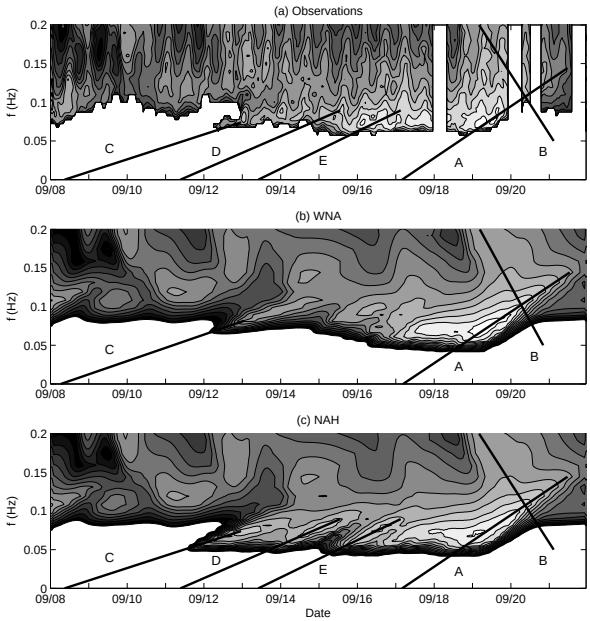

Fig. 4: Time series of one-dimensional wave energy spectra vs. frequency at buoy 44018. Slanted ridges indicate the arrival of swell.

A comparison between diagrams representing measurements, WNA and NAH data (upper, middle and lower panel in Figure 4, respectively) shows that, prior to the arrival of the main swell and local wave fields generated by the storm (ridges A and B), the NAH model was able to reproduce three events (marked C, D and E) that were either completely missed or severely underestimated by the WNA model. (Note that the semi-diurnal, tide-induced periodic fluctuation of spectral wave energy is not reproduced by model data because wave-current interactions are not yet accounted for.)

3 MOVING GRID MODEL

A moving grid version of the WAVEWATCH III model has recently been developed for simulating wave conditions near tropical cyclones. This moving grid version is set up for deep waters, without coastlines. The adopted approach allows a relatively small high resolution, storm-centered grid to be moved with the tropical cyclone.

The moving grid approach provides a natural way to use high resolution wind field analyses for hurricanes in wave modeling. Such modeling efforts are usually hampered by the fact that these wind fields have excellent spatial resolution, but poor temporal resolution. This will be illustrated here with some practical examples for and idealized storm vortex and for hurricane Lili. Details of these studies are presented in Tolman and Alves (2004).

The moving grid model has been extensively used at NCEP to investigate the sensitivity of hurricane wave prediction to grid resolutions, and possible refinements of numerical approaches and physical parameterizations (including coupling with ocean and atmosphere models). It has also been used to revisit a parametric model for estimating maximum hurricane-generated wave height proposed by Young (1988). Preliminary results of this latter investigation are reported below.

3.a Idealized Hurricane Vortex

An idealized tropical cyclone test case is considered for illustrating the moving grid version of WAVEWATCH III. In this test, the wind field is defined as a Rankine vortex and the model domain of 3000×3000 km is resolved with a spatial resolution of 25 km (123×123 grid points). Spectral resolutions are set as in the most common WAVEWATCH III applications at 25 frequencies (0.042 – 0.42 Hz, with 10% increments) and 24 directions ($\Delta\theta = 15°$). The simulation period covers two days, with initial conditions determined directly from the wind field via an adaptation of the JONSWAP relations (standard WAVEWATCH III initialization).

Wave heights generated by a stationary cyclone are shown in Figure 5a. The figure clearly shows that H_s fields away from the hurricane center are dominated by the Garden Sprinkler Effect (GSE). Results of an identical vortex moving at a constant speed of $\vec{v} = 5$ ms^{-1} to the right (on a wave model grid moving at the same speed) are shown in Fig-

ure 5b.

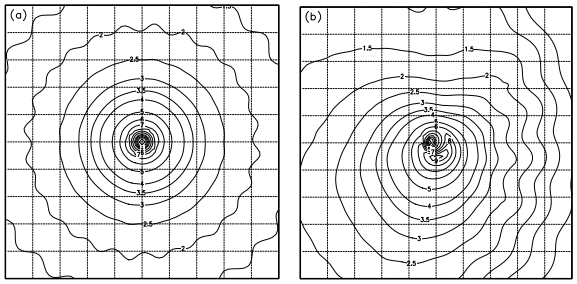

Figure 5: Wave heights (m) from idealized tropical cyclone test. Grid lines at 200 km intervals with storm-centered grid. (a) Stationary cyclone. (b) Cyclone and grid moving with $\vec{v} = 5$ ms^{-1} to the right. Moderate GSE corrections ($\gamma = 2$). [Adapted from Tolman and Alves (2004).]

Relative to the stationary case, the GSE became stronger in the cyclone's propagation direction and nearly disappeared in opposite directions. Stronger GSE is expected in the storm's propagation direction due to the longer retention time within the moving grid of waves ahead of the storm. The reverse is true for waves propagating in the opposite direction, which have lower retention time and thus less GSE.

The GSE effects in the stationary storm case can be alleviated by simply applying the default approach in the WAVEWATCH III model. This consists of smoothing the energy levels of spectral components through spatial averaging, considering neighboring model grid points. The area around each grid point over which the spatial averaging is performed extends in the propagation ($\vec{s}$) and normal ($\vec{n}$) directions as

$$\pm\gamma_s \, \Delta c_g \, \Delta t \, \vec{s} \;\; , \pm\gamma_n \, c_g \Delta\theta \, \Delta t \, \vec{n} \;\; , \qquad (1)$$

where γ_s and γ_n are tunable constants. Details of the method are given in Tolman (2002).

Figure 6a shows the results for the stationary case in which sufficient smoothing was introduced to eliminate the GSE. This required $\gamma_s = \gamma_n = 3.0$. Only marginal effects of the GSE can be observed, and for practical purposes the GSE has been eliminated.

For the moving grid case, the asymmetry of the GSE requires different levels of smoothing in the forward and backward faces of the wave-height field. To solve this problem, a modification to equation (1) is introduced considering that the diffusion factors γ should increase with retention time of wave components within the model grid:

$$\pm\gamma_a\gamma_s \, \Delta c_g \, \Delta t \, \vec{s} \;\; , \pm\gamma_a\gamma_n \, c_g \Delta\theta \, \Delta t \, \vec{n} \;\; , \qquad (2)$$

and

$$\gamma_a = \left(\frac{|\vec{c}_x|}{|\vec{c}_x - \vec{v}|} \right)^p \;\; , \qquad (3)$$

where p is a tuning parameter. For $p = 0$ no correction is applied, whereas for $p = 1$ the averaging area is scaled linearly with retention time.

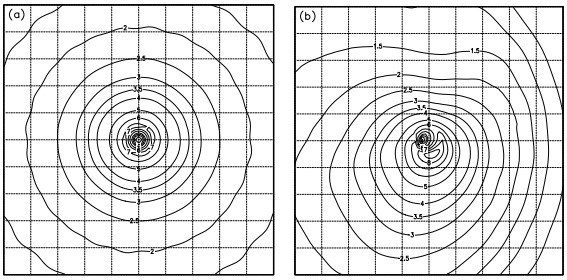

Figure 6: Like Fig. 5 with $\gamma_s = \gamma_n = 3.0$ and $p = 0.5$ in Eqs. (2) and (3). [Adapted from Tolman and Alves (2004).]

Figure 6b shows the results of using the modified smoothing function for a moving vortex using $p = 0.5$. The GSE now is more evenly distributed between the forward and backward faces of the wave-height field than in the case without the grid movement correction (Fig. 5b). As in the stationary case, the GSE effects have been satisfactorily eliminated for practical purposes.

Although spatial smoothing is an efficient way of reducing GSE in numerical wave models, the choice of coefficients requires caution. Smoothing not only eliminates the GSE in the solution away from the vortex's center, but also affects the solution near the center. In fact, a combination of coarse spatial resolution and large averaging coefficients leads to a strong reduction of wave heights. This is illustrated in Figure 7, which shows maximum wave heights versus γ_s and γ_n. By increasing the smoothing factors from 0 to 4, the maximum wave height is reduced by up to 15% on a grid with 25km spatial resolution. Higher resolutions, however, suppress the sensitivity of maximum wave heights to smoothing.

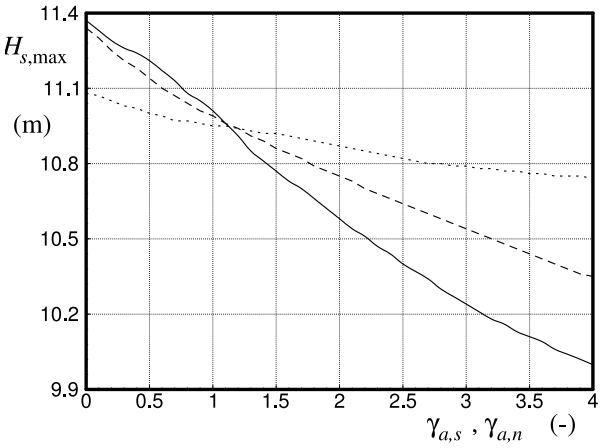

Figure 7: $H_{s,\max}$ (solid line) as a function of γ_s and γ_n, $p = 0$. Dashed and dotted lines: spatial grid resolutions increased from 25 km to 12.5 and 6.25 km. [Adapted from Tolman and Alves (2004).]

3.b Hurricane Lili

An application of the moving grid model to a real case is made considering hurricane Lili's wave fields, in the period between Oct. 1 1800 UTC and Oct. 4 0000 UTC. Forcing winds representing Lili are specified using 3-hourly analyses produced by NOAA's Hurricane Research Division (HRD) of the Atlantic Oceanographic and Meteorological Laboratory (AOML).

To illustrate advantages of the moving grid approach, two wave models are inter-compared: a "conventional" fixed grid model, covering the Gulf of Mexico with a spatial resolution of approximately 10 km; and a model with a 300 km wide grid at the same spatial resolution, centered on the eye of the hurricane. Both models use the spectral resolution as in the previous tests and GSE smoothing factors set to $\gamma_s = \gamma_n = 2.0$. In addition, the moving grid case has $p = 0.5$.

Wind fields for both models are obtained by first interpolating the HRD analyses onto a storm-centered circular grid. These are used directly in the moving grid model, which has also an advection velocity $\vec{v}(t)$ estimated from consecutive track points. Winds for the fixed grid model are obtained by interpolation of the moving grid winds onto track locations in the fixed grid. Fixed grid winds outside the moving circular domain are set to zero. Since analyzed wind fields are generally produced operationally at 6h intervals, two sets with 3- and 6-hourly winds are produced for testing the sensitivity of wave simulations to time resolution of wind fields.

In most operational and practical applications, the internal wave model time step is much smaller than the time resolution of available winds. In the present case, wave model time steps are of the order of 5 min. Consequently, winds have to be internally interpolated. In the moving grid case, winds interpolated to the wave model time step are always storm-centered like in the original wind fields. In a fixed grid, consecutive wind fields 3h or 6h apart are often significantly displaced in space. Interpolation onto higher time resolutions in this case leads to significant spatial aliasing. This is illustrated in the upper panels of Figure 8, which shows winds for both models at a time halfway between two consecutive analyzed wind fields.

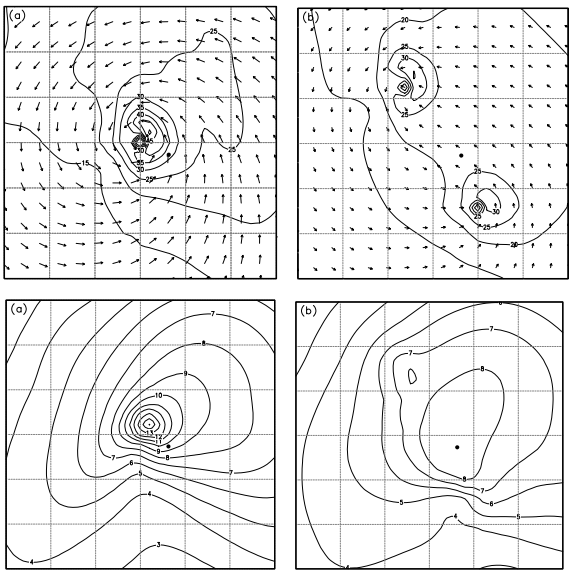

Figure 8: U_{10} in ms^{-1} (upper panels) H_s in m (lower panels) on October 2, 2100 UTC. Interpolated fields for the moving grid (a) and fixed grid (b) models 3h before and after valid time from 6-hourly winds. Grid lines at 50 km intervals, contour lines at 5 ms^{-1} (U_{10}) and 1 m (H_s) intervals. [Adapted from Tolman and Alves (2004).

Lower panels in Figure 8 show wave heights computed at the time of winds presented in Figure 8. Waves in the moving grid model are higher and distributed spatially such that only one wave-height maximum is observed in the front right quadrant, as expected from the forcing wind-field structure. In contrast, waves in the fixed grid model are lower

and display a less consistent spatial distribution, with the development of a new local wave maximum in the northwest quadrant due to the existence of two false storm centers in the interpolated winds shown in Figure 8.

The strong impact of the wind interpolation approach on simulations of wave heights is further illustrated in Figure 9, presenting time series of maximum winds and wave heights. In the moving grid model, 3- or 6-hourly winds are very closely related, both producing very similar wave height maxima. In the fixed grid model, maximum wind speeds at times coinciding with available analysis times are close to the moving grid values, but fall to unrealistically low values at interpolated times. These lower maximum wind speeds, which reflect the spatial aliasing shown in Figure 8, result in significantly lower maximum wave heights, as shown in Figure 9b.

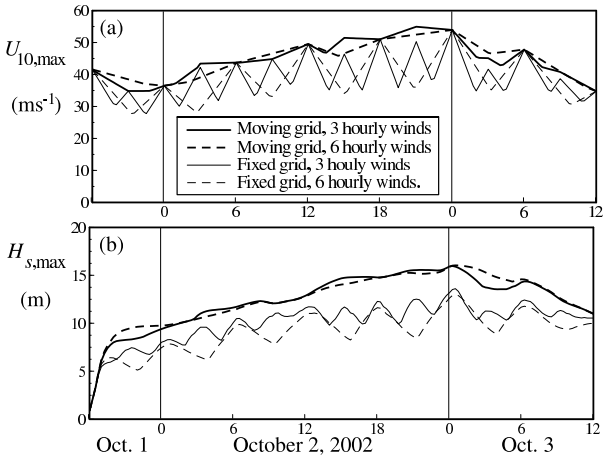

Figure 9: Maximum U_{10} (a) and H_s (b) from the moving and fixed grid models for 3- and 6-hourly wind fields.

Most operational wave models use input winds with time resolutions much larger than their internal time steps. Therefore, spatial aliasing is expected to occur when simulating waves generated by rapidly changing storms. This problem can be reduced if winds with higher time resolutions are used. Such is the case of NCEP's two operational models for predicting hurricane-generated waves, NAH and NPH, which use hourly winds from the GFDL model.

Results above suggest that winds at higher time resolutions can be generated when only coarse resolution analyses are available (say, at 3h or 6h intervals) by first interpolating storm winds on a storm-centered (moving) grid to the desired time resolution. Then, interpolating these storm-centered winds back onto the fixed grid at given storm track locations. Simulations made with such winds produce maximum wave heights much closer to the moving grid model results (figure not shown).

4 MAXIMUM HEIGHT PREDICTIONS

Several practical approaches are presently used for estimating maximum wave heights generated by hurricanes. The most popular consist of parametric models developed on the basis of numerical modeling of wave evolution under hurricane forcing. An example is the parametric model proposed by Young (1988) [henceforth Y88], which has been widely used in emergency management, contingency plans and forecast guidance worldwide.

According to Y88, a major limitation of his parameterization for maximum hurricane waves is the use of simulations made with a second-generation wave model. In that sense, Y88 argues that although his proposed parametric model may be successful in practical applications, a more refined parameterization with a broader range of applications requires simulations made with a third-generation wave model.

In this section we present preliminary results of a study made to refine the Y88 parametric model. This refinement is achieved by using simulations of hurricane-generated wave fields made with the moving-grid version of the third-generation wave model WAVEWATCH III, which is described in section 3.

4.a Conceptual Framework

The Y88 parametric model is essentially an adaptation of the JONSWAP fetch-limited growth relationship (Hasselmann et al., 1973) made for the purpose of predicting hurricane-generated H_s^{max}. In the original JONSWAP relations, values of H_s are estimated as a function of fetch X and a representative wind speed U.

Following the approach introduced by Bretschneider (1957), the parametric model of Y88 estimates hurricane-generated maximum wave heights H_s^{max} by replacing the actual fetch X by an equivalent fetch X_{eq}. This quantity is defined as a function of

three wind field parameters which ultimately determine the magnitude of H_s^{max}: the forward advection velocity of the storm V_{fm}, the maximum wind speed U_{max} and the radius of maximum winds R.

The relation between H_s^{max} and X_{eq} is identical to the JONSWAP equation:

$$\frac{gH_s^{max}}{U_{max}^2} = \alpha \left(\frac{gX_{eq}}{U_{max}^2} \right)^{\beta}. \tag{4}$$

In the original equation for a fetch-limited wave growth scenario, the wind field is quasi-homogeneous and X_{eq} is is simply the downwind distance along a straight line, starting at a point where the waves are negligibly small (e.g., a coastline). In a moving storm, X_{eq} should represent (i) the distance over which U_{max} effectively contribute to wave growth (no longer a straight line), and (ii) the added growth due to an "extended fetch" effect, resulting from waves moving forward with the storm.

In the Y88 parametric model, V_{fm} and U_{max} are the basic equivalent fetch parameters, while R_{max} is a scaling parameter representing the relative size of the hurricane system. Initial X_{eq} values are determined from (4) by using H_s^{max} calculated from model simulations using a range of U_{max} and V_f and a fixed reference R_{max}^{ref}.

The equivalent-fetch relationship valid only for the chosen R_{max}^{ref} is defined as a second-order polynomial P_{ref}, with coefficients determined by fitting V_{fm} and U_{max} to X_{eq}^{ref} (here the subscript ref is used to label equivalent fetches from simulations using R_{max}^{ref}). Simulations made with a range of other values for R_{max} are then used to provide a scaling law for the polynomial expression, providing a generalized equivalent-fetch relationship in the form:

$$\begin{aligned} \frac{X_{eq}}{R'} &= a_f U_{max}^2 + b_f U_{max} V_{fm} + \\ & c_f V_{fm}^2 + d_f U_{max} + e_f V_{fm} + f_f, \end{aligned} \tag{5}$$

where a_f, b_f, c_f, d_f e_f and e_f are the coefficients of P_{ref} normalized by R_{ref}, and the effective radius R' is introduced as the functional relationship $R' = f(R_{max})$. This functional relationship is expressed as:

$$R' = a_r \log R - b_r. \tag{6}$$

Coefficients a_r and b_r are also determined by curve fitting. First, values of X_{eq} are obtained directly from equation (4) using simulated quantities. Second, a functional relationship between the ratios X_{eq}/X_{eq}^{ref} and R_{max}/R_{max}^{ref} is established. Y88 argues that such relationship can be well approximated by:

$$\frac{X_{eq}}{X_{eq}^{ref}} = \alpha \log \left(\frac{R_{max}}{R_{max}^{ref}} \right) + 1, \tag{7}$$

with α determined by curve fitting. This leads to the definition of expressions for the coefficients a_r and b_r:

$$\begin{aligned} a_r &= \alpha R_{max}^{ref} \\ b_r &= R_{max}^{ref} \left(\alpha \log R_{max}^{ref} - 1 \right). \end{aligned} \tag{8}$$

In Y88, coefficients in (5) and the functional form of R' are determined from simulations using a second-generation wave model. Data in Y88 give $a_r = 22.5 \times 10^3$ and $b_r = 70.8 \times 10^3$. In the present study, the polynomial coefficients in eqn. (5) and in (6) are re-derived by fitting V_{fm} and U_{max} to X_{eq}, estimated from H_s^{max} computed using the third-generation model WAVEWATCH III.

In a quest for improvements to the original parametric Y88 model, our analysis is extended to investigate if there is any benefit in rewriting the basic equation for X_{eq}. This is done by assuming that the equivalent fetch depends directly on R_{max}, as initially suggested by Ross (1976). To this initial suggestion, we add the general consensus that X_{eq} should also depend on V_f and U_{max}, and introduce the hypothesis that the cumulative fetch effect should also depend on the group speed of dominant waves c_g^{max}.

In other words, R_{max} is taken as a proxy for the wind field curvature, assumed to be important in determining the geometry of the effective fetch in a circular wind field, which will also be determined by V_f and U_{max}. As argued by Y88, the effectiveness of the storm advection speed V_f in developing a cumulative fetch effect will depend on c_g^{max}, the speed in which the dominant wave energy is traveling.

Reflecting this alternative conceptual framework, a new equivalent fetch definition is proposed:

$$\chi = \left[R_{max} \left(1 + \gamma V_f / c_g^{max} \right) \right]^{\lambda}, \tag{9}$$

where γ and λ are determined from curve fitting to simulated values of H_s^{max}. A general formula consistent with the Y88 parametric model, which relates back to the JONSWAP growth curve would then be

$$X_{eq} = a\chi^b, \tag{10}$$

with a and b obtained by fitting the resulting form of χ to the JOSNWAP growth curve.

For the purpose of obtaining optimal parameter values in (9) and (10), an initial guess for c_g^{max} is obtained from U_{max} by using the reanalyzed asymptotic Pierson-Moskowitz peak frequency (Alves et al., 2003):

$$f_p = \frac{g}{U_{max} 0.123} \tag{11}$$

A more accurate value of c_g^{max} and a final form for (9) and (10) are obtained through a small number of iterations, using a modification of the JONSWAP relation for f_p:

$$2\pi f_p = \frac{g}{U_{max} \alpha_J X_{eq}^{\beta_J}}. \tag{12}$$

In a practical forecasting application, c_g^{max} may be estimated by using first (11) and then repeatedly (12) until values of χ and X_{eq} are stabilized to a desired level of accuracy.

4.b Simulating Waves in Hurricanes

Simulations of wave growth under hurricane forcing conditions were made using the WAVEWATCH III model, Beta version 3.04. WAVEWATCH III is different from the second-generation model used in Y88 in many aspects, including all parameterizations of physical processes, numerical schemes for solving propagation and integrating source terms, code architecture etc. The first most crucial difference, however, is in their treatment of the nonlinear wave-wave interactions source function.

In second-generation models, nonlinear wave-wave interactions are estimated via simplified formulations. As a consequence, high-frequency energy fluxes at high-frequency components, which are typically strong in hurricane wave spectra with broad directional spread, are not properly accounted for. It is believed this problem is minimized in third-generation models due to the presence of a nonlinear interactions source term that has, in theory, the same number of degrees of freedom as the wave spectrum itself.

A second major difference between the present modeling approach and that of Y88 is in the setup of spatial grids. Y88 had two fixed nested grids with resolutions set at 30km and 15km. In the new framework, the use of a spatial grid moving with the storm allowed computations using a single grid with 0.1° resolution (around 10km), covering the entire area under direct influence of hurricane winds. This also allowed to keep all model properties unchanged relative to the forcing wind fields. The model setup included a spectral grid with 25 frequencies ranging from 0.04Hz to 0.41Hz and 36 directions.

Surface wind fields representing a hurricane vortex were specified by a modified Rankine vortex model (Phadke et al., 2003):

$$U = U_{max} \left(\frac{r}{R_{max}} \right)^s, r < R_{max};$$
$$U = U_{max} \left(\frac{R_{max}}{r} \right)^s, r \geq R_{max}, \tag{13}$$

with r the distance from the storm center and s a shape parameter set to 0.6. Winds were adjusted to include the observed curvature of wind vectors toward the center of the storm, following the NOAA/NWS standard project hurricane (Phadke et al., 2003). Adjustments varied linearly between 10° and 20° from the storm center to R_{max}, increasing linearly to 25° at $1.2R_{max}$ and remaining constant at 25° elsewhere.

Final corrections to surface wind fields included the effects of storm advection. For this purpose, the equation accounting for forward storm motion used in the SLOSH storm-surge model, as outlined in Jelesnianski et al. (1992), was adopted:

$$\mathbf{dU} = \mathbf{V_f} \frac{R_{max} r}{R_{max}^2 + r^2}, \tag{14}$$

where the vector correction $\mathbf{dU}$ is added to radial wind speeds obtained from (13).

More than 200 simulations were made with the following characteristics:

- 20m/s $\leq U_{max} \leq$ 60m/s, with 10m/s intervals;
- 0m/s $\leq V_F \leq$ 10m/s, with 2.5m/s intervals;
- R_{max} equal to 20km, 30km, 50km and 80km.

Maximum H_s values were extracted from the last time-slice output of each simulation. Durations of

Table 2: Parameter values for equation (5) and (6) obtained from FQS and Y88 data.

Run	a_f	b_f	c_f	d_f	e_f	f_f	a_r	b_r
Y88	-2.175×10^{-3}	1.506×10^{-2}	-1.223×10^{-1}	2.190×10^{-1}	6.737×10^{-1}	7.980×10^{-1}	22.5×10^{3}	70.8×10^{3}
FQS	5.936×10^{-5}	1.719×10^{-2}	-3.479×10^{-2}	8.555×10^{-2}	1.319×10^{-1}	-5.340×10^{-1}	29.7×10^{3}	103.7×10^{3}

runs were defined as a function of U_{max}, varying between 5 and 9 days. Tests were also made to verify the sensitivity of results to the angle of the wind vectors and to the position of the maximum wind region (front or rear quadrant).

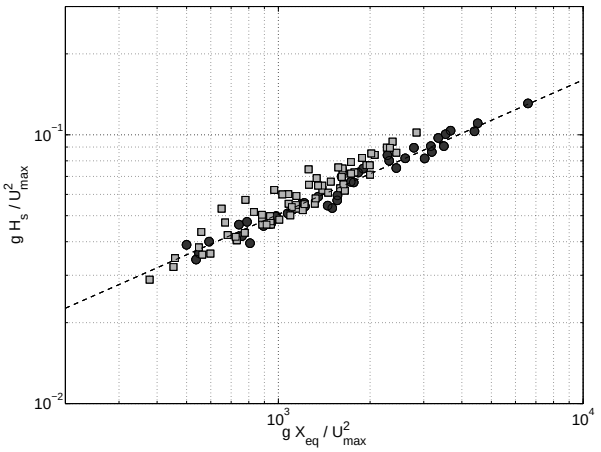

Figure 10: Nondimensional H_s vs. X_{eq}: comparison of estimates made with new coefficients (■) against data from Y88 (•). The JONSWAP fetch-limited growth curve (dashed line) is also plotted for reference.

4.c Parametric Model Revisited

Preliminary results presented in this section focus on simulations made with synthetic hurricane vortices with maximum winds in the front quadrant. This configuration reproduces more closely the wind forcing conditions used by Y88. Therefore, we make an assessment of changes to parametric model coefficients and form due to the use of (i) a new numerical model and (ii) an experimental framework featuring a movable spatial grid. Results from other experiments, which included maximum winds in the rear quadrant and changes in the wind vector angle, will be explored in more detail in a forthcoming paper.

Following the procedure of Y88, front quadrant simulations [henceforth FQS] produced a new set of coefficients in equations (5) through (9), which are compared to the values proposed by Y88 in Table 2. New values for e_f were found to have a greater impact in terms of differential performance of equation (4). The new value for e_f makes the parametric model less sensitive to V_f when compared to the results of Y88.

Figure 10 presents a plot of nondimensional H_s against estimates of X_{eq} made with equation (4) and the new coefficients obtained from FQS runs. The data used by Y88 and the JONSWAP fetch-limited growth curve are also plotted for comparison. The Y88 H_s^{max} data fits generally well the JONSWAP curve, with an RMS error of 5%. H_s^{max} data from the new simulations also fit generally well the JOSWAP curve, but with a higher RMS error of 12%.

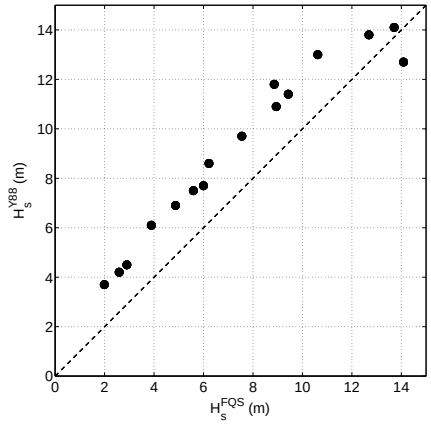

Figure 11: H_s from Y88 and FQS runs. Values of H_s are co-located at identical U_{max}, V_F and R_{max}.

Data in Figure 10 from both series of experiments made presently and by Y88 indicate further differences between models, which may significantly impact the predictive skill of a parametric model. For instance, both sets of experiments use similar ranges for V_f, U_{max} and R_{max}. However, data from Y88 produce H_s that is generally higher, as illustrated in Figure 11. Note an almost contant positive bias of 2m in the Y88 data relative to H_s from the FQS runs, at wave heights smaller than 13m.

FQS results indicate that H_s^{max} generated with the WAVEWATCH III model do not support a para-

metric model in the form (4) as strongly as the Y88 data, as seen in Figure 10. Data from these new simulations provide more solid support to the alternative parametric model form defined by equation (9), as seen in Figure 12. The fit of H_s^{max} FQS data is significantly improved relative to the Y88 model: the RMS error is now below 2.5%.

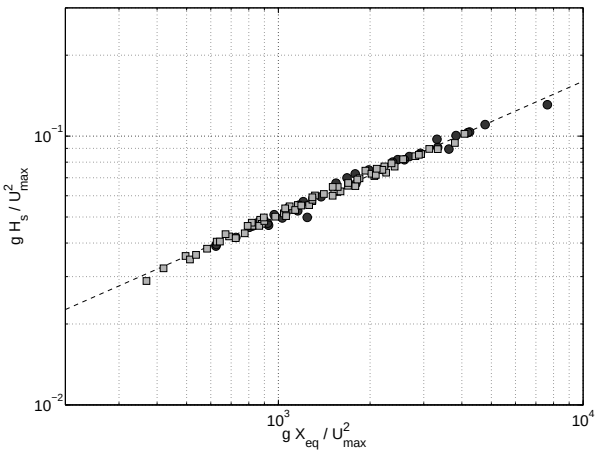

Figure 12: Nondimensional H_s vs. X_{eq} computed using eqn. (9) and (10): comparison of estimates made with FQS (■) and Y88 (•) data. The JONSWAP fetch-limited growth curve (dashed line) is also shown.

Figure 12 also shows that the Y88 H_s^{max} data supports the new parametric form defined by equations (9) and (10). The fit of these data to the new model is also improved compared to the Y88 parametric model form, as indicated by a RMS error or 3.9%. Table 3 provides parameter values of the new parametric form obtained from these preliminary results.

Table 3: Preliminary parameter values for equations (9) and (10) obtained from FQS and Y88 data.

Run	γ	λ	a	b
Y88	2.3	0.5	1106.1	0.76
FQS	2.1	2.8	0.6	0.29

Most of the relatively larger scatter of FQS data fitted to the Y88 model form in Figure 10, results from the fact runs with different R_{max} do not seem to support the scaling law (6) proposed in Y88. By incorporating R_{max} into the basic parametric model form, equations (9) and (10) lead to a closer fit of model H_s and their corresponding equivalent fetch values to the JONSWAP growth curve. This benefit is also seen when Y88 data is considered.

Results presented in this section are preliminary. Their purpose is exclusively to provide a first view of how third-generation model simulations impact the form and structure of a parametric hurricane-generated wave prediction model. A more thorough investigation, including results from an extended set of simulations, will be presented in a forthcoming paper. Such investigation will also present a detailed performance assessment of the different approaches outlined above using measurements of hurricane-generated maximum significant wave heights.

References

Alves, J.H.G.M., M.L. Banner and I.R. Young, 2003: Revisiting the Pierson-Moskowitz asymptotic limits of fully-developed wind waves. *J. Physical Oceanography*, **33**, 1301-1323.

Bretschneider, C.L., 1957: Hurricane design wave practices. *J. Waterw. Harb. Div.*, **83**(WW2), 1238.1-1238.33.

Chao, Y.Y., J.H.G.M. Alves and H.L. Tolman, 2004: An Operational System for Predicting Hurricane-Generated Wind Waves in the North Atlantic Ocean. *Weather and Forecasting*. Submitted.

Donelan, M. A. and Pierson, W. J., 1983, The Sampling Variability of Estimates of Spectra of Wind Generated Gravity Waves, *J. Geophys. Res.*, **88**(C7), 4381-4392.

Hasselmann et al., 1973: Measurements of wind-wave growth and swell decay during the Joint North Sea Wave Project (JONSWAP). *Dtsch. Hydrogr. Z.*, Suppl. A, **8**(12), 95p.

Jelesnianski, C.P., J. Chen and W.A. Shaffer, 1992: SLOSH: Sea, lake and overland surges from hurricanes. *NOAA Tech. Rep.*, NWS-48, 317p.

Phadke, A.C, C.D. Martino, K.F. Cheung and S.H. Houston, 2003: Modeling of tropical cyclone winds and waves for emergency management. *Ocean Engng.*, **30**, 553-578.

Ross, D., 1976: A simplified model for forecasting hurricane-generated wind waves. *Bull. Am. Meteorolog. Soc.*, **57**(1), 113.

Tolman, H.L., 2002: Alleviating the Garden Sprinkler Effect in wind wave models. *Ocean Modelling*, **4**, 269-289.

Tolman, H.L., B. Balasubramaniyan, L.D. Burroughs, D.V. Chalikov, Y.Y. Chao, H.S. Chen, and V.M. Gerald, 2002: Development and implementation of wind generated ocean surface wave models at NCEP. Weather and Forecasting, 17, 311-333.

Tolman, H.L. and J.H.G.M. Alves, 2004: Numerical modeling of wind waves generated by tropical cyclones using moving grids. *Ocean Modeling*. In press.

Tolman, H.L., J.H.G.M. Alves and Y.Y. Chao, 2004a: A review of operational forecasing of wind generated waves by hurricane Isabel at NCEP. *NOAA/NWS/NCEP/MMAB Technical Note*, **235**, 45p.

Tolman, H.L., J.H.G.M. Alves and Y.Y. Chao, 2004b: Operational forecasting of wind generated waves by hurricane Isabel at NCEP. *Weather and Forecasting*. Submitted.

Young, I.R., 1988: A parametric hurricane wave prediction model, it J. Waterw. Port Coastal Engng., **114**, 637-652.